Classical harmonic generation in rare gases

Raam Uzdin* and Nimrod Moiseyev
Department of Physics, Technion, Israel Institute of Technology, Israel
(Received 4 December 2009; published 8 June 2010)

The classical microcanonical ensemble approach to high-harmonic generation (HHG) in rare gases subjected to intense laser fields is studied. We show that the ensemble spectrum is a "sampled" version of the single trajectory spectrum. Unlike the radiation of the single ensemble member, the total ensemble radiation possesses all the basic HHG features: odd laser harmonics, plateau, and cutoff. The sampling theorem for uniform grids is used to explain why the ensemble spectrum can be computed accurately with a very small number of ensemble members compared to the Monte Carlo method. Furthermore, The phase space relevant to harmonic generation is found to be significantly smaller than the field free microcanonical ensemble. In addition we demonstrate the seeding effect that was predicted and observed in quantum simulation. For circular polarization, we verify that the harmonic generation is highly suppressed even when the argument of the three-step model does not apply. All the findings are numerically calculated for the xenon atom.

DOI: 10.1103/PhysRevA.81.063405 PACS number(s): 32.80.Wr, 42.65.Ky

I. INTRODUCTION

High-harmonic generation (HHG) has been an active field of research for the last 20 years [1–3]. Experimentally it was observed that rare-gas atoms subjected to intense laser pulses can emit light in frequencies which greatly exceed the several first harmonics [4–6]. In fact, harmonics beyond 100 were observed. Such high harmonics are qualitatively well explained by the three-step model (also known as the "simple man model") conceived by Corkum [7] and formalized by Lewenstein *et al.* [8]. In short, this model assumes a fraction of the wave-function tunnels outside the joint potential of the atom and driving laser. Then, driven by the laser field, the escaped wave packet repeatedly collides with the core and creates high harmonic radiation. The propagation of the wave packet outside the atomic potential is calculated using the classical equation of motion. Semiclassical propagator methods have also been successfully used [9] to calculate the spectrum in this regime (see [2] for more methods). In this article, however, we consider low enough intensities so that tunneling effects are not so dominant. The Keldysh parameter in our model is roughly 2, contrary to the three-step model where it is much smaller than unity.

The classical microcanonical ensemble approach of Leopold and Percival [10] has been used successfully in the past for calculating atom ionization rates in laser fields [10] and for describing atomic and molecular dynamics ([11] and references therein). In the microcanonical approach, the ensemble contains all the trajectories (or initial conditions) of a classical electron orbiting the atom with the same energy. This energy is taken to be the quantum ground-state energy (field free). Finally, ensemble integration over all possible different initial conditions is carried out using the Monte Carlo method. Each trajectory corresponds to a different realization so the trajectories do not interact with each other. This scheme was also applied to the calculation of HHG radiation [11–15]. In HHG, the radiation spectrum of a single member of the ensemble (i.e., a single classical electron trajectory of an electron-atom-laser system) contains features which are not observed either in quantum simulation [16] or in experiments [4,5]. Yet, after the ensemble average is taken and the radiation from all possible trajectories (ensemble members) is coherently summed, the unobservable features vanish and the typical HHG features (plateau, cutoff, and odd harmonics) emerge quite clearly.

The main purpose of this article is to isolate this "ensemble effect" and determine what is the simplest and smallest subensemble for which only the observed HHG features appear. Since only bound, nonchaotic trajectories are considered, this classical description is limited to the part of the spectrum which is dominated by the bound states. The three-step cutoff associated with ionization and recombination, for example, cannot be obtained from this model. Nonetheless the model provides interesting insights into the classical nature of harmonic generation. Comparison to the quantum spectrum is left for future work where different alternatives of choosing and combining these subensembles and other subensembles need to be considered.

This paper is organized as follows. The next section describes the physical model, the assumptions made, and the methods used to acquire the solution. Section III starts by presenting the relation between the seemingly disordered single member HHG spectrum and the structured HHG spectrum of the ensemble average. The calculation is carried out for a specific subensemble whose members all move on the same circle around the nucleus in the absence of a driving laser. Then in Sec. III B the effect of the circle's radius value is examined. We find that there is a small number of distinct radii that give rise to significant HHG spectra. Section III C discusses the implication of the sampling theorem and sheds some light on the convergence of the result with so few integration points. This part is unique to our approach which is based on an evenly spaced grid and not on the Monte Carlo method. In the last two subsections, our approach is applied to some more complex physical scenarios. In Sec. III D the seeding effect [17], which was predicted and demonstrated using quantum theory and quantum simulation, is shown to appear quite clearly already at the classical level. We finish Sec. III by applying the model to the circular polarization case and find that there is no HHG

*raam@tx.technion.ac.il

 ©2010 The American Physical Society

radiation. Even though this result is expected, the mechanism responsible for it is rather different from that of the three-step model. Finally, in Sec. IV we conclude.

II. METHOD

A. Ensemble description

One can consider the ensemble of Leopold and Percival as a different realization of a single atom or as a statistical description of many atoms. We adopt the first point of view. The circular ensemble is defined in the following way: Let all ensemble members be aligned so that the axis of rotation is along z. The laser pulse polarization is along x and the field-free initial conditions of the electron in the ith member are

$$\begin{aligned} x_i(t=0) &= r_0 \cos\varphi_i, \\ y_i(t=0) &= r_0 \sin\varphi_i, \end{aligned} \tag{1}$$

where φ_i is the initial azimuthal angle of the electron in the ith member (later on we drop the index i but it is assumed that different φ values correspond to different members). r_0 is the field-free radius, which is the same for all members. The reason for this specific laser-atom orientation is that quantum simulations [16] have shown that this alignment's HHG spectrum is considerably stronger than that of other orientations. If ensemble members are allowed to be oriented in the $-z$ direction as well, then by symmetry the x component of the motion stays the same, but the y component changes its sign. This leads to a cancellation of the y polarization, but the x (driving) polarization is left unchanged. For this reason it is enough to consider just the $+z$ orientation, and keep in mind that the total induced dipole is only in the x direction.

Velocities are chosen so that in the absence of a laser field, a closed circular trajectory of radius r_0 is produced; i.e., the field-free (ff) solution of x_i is

$$x_{i,\mathrm{ff}} = r_0 \cos(\omega_{\mathrm{ff}} t + \varphi_i), \tag{2}$$

where the field-free rotation frequency ω_{ff} is given by $\omega_{\mathrm{ff}}^2(r_0) = \frac{1}{r_0}\frac{\partial V}{\partial r}\big|_{r_0}$. ω_{ff} should not be confused with $\omega_{\mathrm{rotation}}$ which is the electron rotation frequency "dressed" by the external field. In principle, elliptical orbits should also be included. We observe, though, that in the parameter space explored in this work, even mild ellipticity causes the trajectory to immediately ionize. Nevertheless, it is not claimed that orbits with small enough ellipticity, especially the ones which are close to the core, do not contribute to the HHG spectrum. Even though some argument in favor of this simple "circular ensemble" have been given, we recall that the main motivation is to study the simplest case for which the "ensemble effect" takes place.

B. The equations of motion

The equations of motion are

$$\begin{aligned} \ddot{x} &= -\frac{\partial V(r)}{\partial x} + A(t)\sin(\omega_L t), \\ \ddot{y} &= -\frac{\partial V(r)}{\partial y}. \end{aligned} \tag{3}$$

$V(r)$ is the atomic field-free potential, $A(t)$ is the slow varying envelope of the laser pulse, and ω_L is the laser frequency. Each atom has only a single active electron. The equations of motion are solved using the Runge-Kutta 45 method. For $V(r)$ we use the Xe $5p$ Hartree-Slater potential, which takes into account the effect of the other electrons in the atom on the valence electron. Even though a single classical orbit does not model the $5p$ level, the $5p$ Hartree-Slater potential is used to simulate the potential the single active electron experiences in the inner shells of the atom.

The driving laser pulse parameters are the following. The laser frequency is 0.0925 a.u. (krypton fluorine) and the pulse duration is about 200 optical cycles (~0.3 ps). The envelope of the pulse is super-Gaussian of power 4. Finally, for a nonrelativistic motion, the radiation is proportional to the acceleration of the charge. Thus, the spectrum is the Fourier transform of the acceleration $\ddot{x}$. In the calculation of the spectrum, a Blackman window is used to suppress the effects of side lobes (this is of particular importance for the single member spectrum where the acceleration is not zero at the edge of the calculation window).

We use $S(\omega)$ or $S(\omega,\varphi)$ when needed for the single member (complex) spectrum, and $C(\omega)$ for the averaged collective ensemble (complex) spectrum. The averaged collective ensemble spectrum *power* is

$$|C(\omega)|^2 = \left|\frac{1}{2\pi}\int_0^{2\pi} S(\omega,\varphi)d\varphi\right|^2. \tag{4}$$

For the spectrum, we take all the signal including the turn on and turn off and not only the stationary parts of it (unlike [16]). This test is more strict than when considering only the flat part of the pulse.

C. Hyper Raman lines

The radiation spectrum of a classical electron orbiting the nucleus while being driven by an external laser field shows a strong presence of the "dressed" electron rotation frequency, $\omega_{\mathrm{rotation}}$. Due to the nonlinearity of the equation of motion for a nonharmonic potential, combinations of $\omega_{\mathrm{rotation}}$ and ω_L (hyper Raman lines [18] or satellites [12]) also appear. For the classical one-dimensional anharmonic oscillator in very strong fields, it has been shown [18] that dissipation highly suppresses the hyper Raman lines while hardly affecting the laser harmonics. Unfortunately, it is not clear what is the physical source of dissipation in a basic classical atom-laser system.

In spite of that, this work shows that the strong dependence of the hyper-Raman-lines phase on the initial conditions, leads to their mutual cancellation when the total ensemble radiation spectrum is calculated.

III. RESULTS

A. The relation between single member spectrum and ensemble spectrum

Figure 1 shows the numerical calculation of an HHG spectrum for the parameters given in Sec. II B and a laser pulse peak intensity of 6×10^{13} W/cm^2.

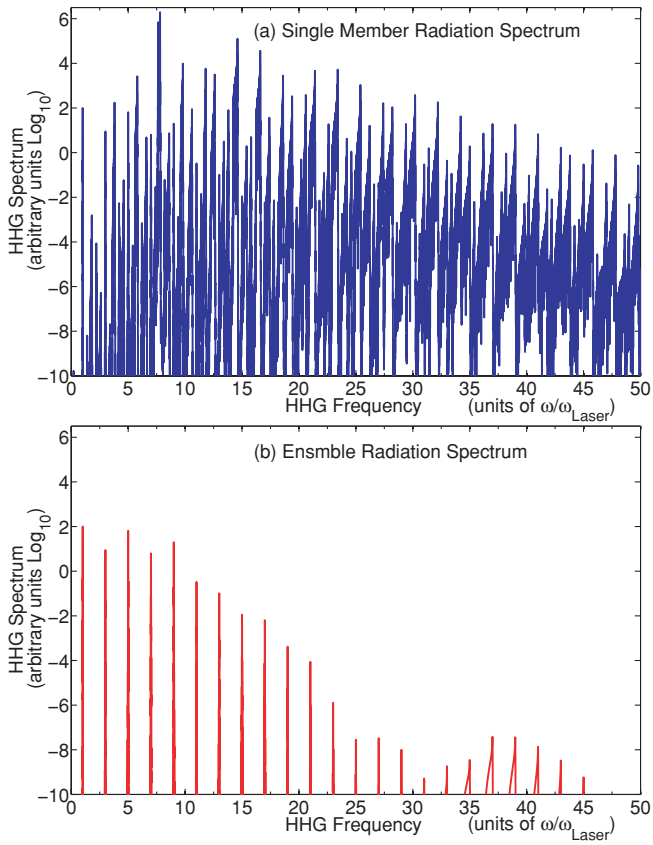

FIG. 1. (Color online) (a) A typical HHG radiation spectrum generated by a classical electron trajectory in an atom driven by a laser field. The spectrum contains many hyper Raman lines which are combinations of the laser frequency and the electron rotation frequency. (b) HHG averaged radiation spectrum of a classical trajectories ensemble. The ensemble average filters out all the unobserved hyper Raman lines and leaves only the odd laser harmonics. The ensemble averaged spectrum shows the three basic HHG features: odd laser harmonics, plateau, and cutoff.

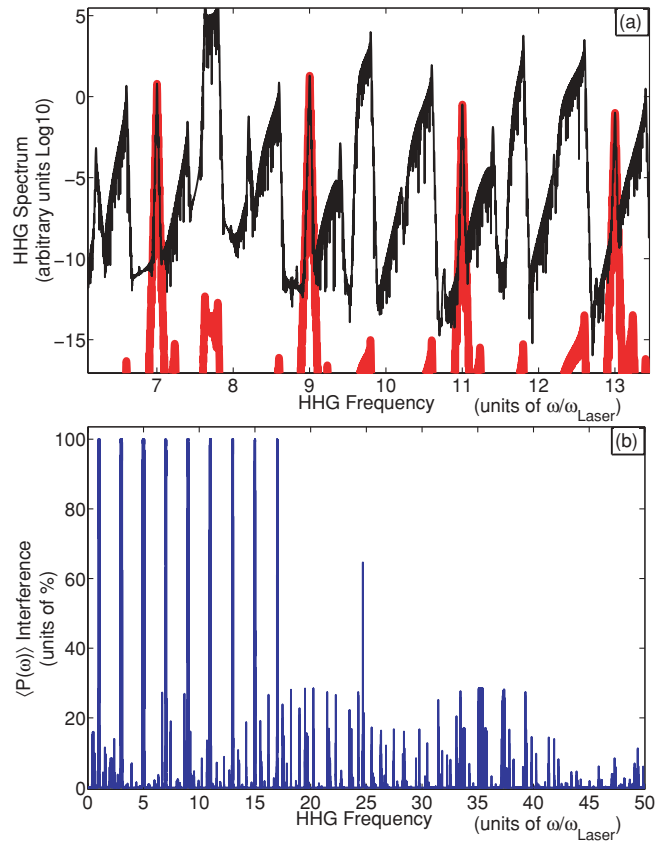

FIG. 2. (Color online) (a) The thick red curve is a zoom-in on Fig. 1(a). The thin black curve is a zoom-in on Fig. 1(b). The ensemble HHG spectrum (thick red) in the plateau zone is a sampled version of the single member HHG spectrum (thin black) at odd laser harmonics. (b) Using the normalized spectrum $\langle P(\omega)\rangle$ [see Eq. (5)], one can see that all ensemble members are in phase just for odd laser harmonics, while they destructively interfere for other frequencies.

For each value of φ, corresponding to a different member or realization in the ensemble, the spectrum $S(\omega,\varphi)$ is calculated. A typical $S(\omega,\varphi)$ is plotted in Fig. 1(a). Next, the ensemble average of the acceleration along x is calculated, and its Fourier transform, the ensemble average spectrum $|C(\omega)|^2$, is plotted in Fig. 1(b).

We make the following observation:

(1) The single member spectrum $S(\omega)$ can contain any combination of the laser frequency and the rotation frequency (i.e., hyper Raman lines).

(2) Only odd laser harmonics appear in the ensemble spectrum $C(\omega)$.

(3) Only in $C(\omega)$ does a plateau and cutoff appear in the spectrum. In contrast, $S(\omega)$ decays far too slow to agree with typical observed or calculated spectra.

Even in such a simple ensemble, all the basic HHG features appear. The essence of the observed plateau is a nonlinear effect; decreasing the laser intensity by a factor of just 4 causes a fast linear decay (on a log scale) in the spectrum with no plateau. Next we wish to see the relation between the single member and ensemble spectra, and study the cause of cancellation of all frequencies which are not odd laser harmonics. Figure 2(a) shows the single member (thin black) and ensemble (thick red) spectra. This is simply a magnified combined version of Figs. 1(a) and 1(b). One can see how $C(\omega)$ "samples" $S(\omega)$ at the odd harmonic frequencies below the cutoff. Actually we observe that the absolute value of $S(\omega,\varphi)$ is practically φ independent. The phase structure, however, is very sensitive to φ. To probe this dependence, it is useful to define the "normalized spectrum" $P(\omega,\varphi) = S(\omega,\varphi)/|S(\omega,\varphi)|$. We selected 100 φ values uniformly distributed in the interval $[0,2\pi]$, calculated their normalized spectrum and plotted the ensembles normalized spectrum:

$$\langle P(\omega)\rangle = \sum_i S(\omega,\varphi_i)/|S(\omega,\varphi_i)|. \tag{5}$$

Figure 2(b) shows how perfect constructive interference occurs only at the odd laser harmonics frequencies, and that the interference is destructive elsewhere. For $\omega = (2n+1)\omega_L$, $S(\omega,\varphi_i)$ is in phase with the driving field regardless of initial condition φ_i. Above the cutoff there is no longer constructive interference even at the odd laser harmonics. Note that the mechanism responsible for the cutoff and odd harmonics in this system is completely different from that of the three-step model.

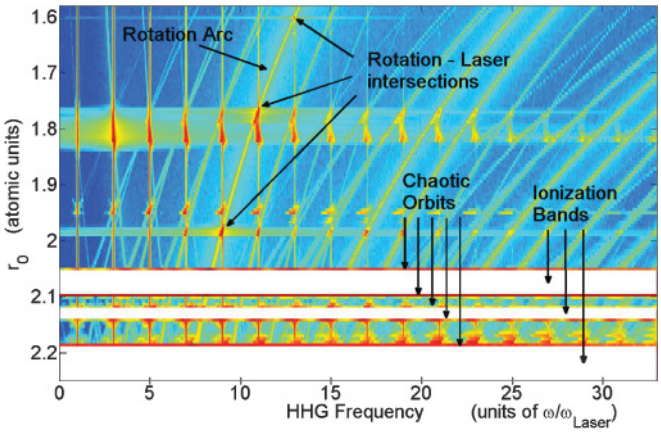

FIG. 3. (Color online) HHG ensemble spectrum for different initial (field-free) radii. The y axis is the distance from the nucleus, r_0, and the x axis is the frequency in units of the laser frequency. The color map is logarithmic. The white bands are ionized trajectories. The main arc is the (dressed) electron rotation frequency, and the vertical lines are odd laser harmonics. While low harmonics appear for any radius, only a few give rise to high harmonics. Some of these points happen when the "rotation arc" crosses a harmonic line. This is a direct consequence of the effect shown in Fig. 2 (see text). The classical "hot spots" of harmonics generation are sparse and constitute less than 3% of the possible initial conditions.

B. HHG contributions from different initial field-free radii

After examining a specific r_0 ensemble, it is interesting to see what impact the value of the initial field-free radius might have. At this point it is not clear if all radii contribute roughly the same or if there are some preferred radii which are considerably more dominant. For that purpose we calculated $C(\omega)$ for different field-free radii, r_0. In Fig. 3, each row is the ensemble spectrum of a different r_0. The y axis is the initial field-free distance from the nucleus (atomic units), and the x axis is the frequency (in units of the laser harmonics). For clarity it is highly recommended to view the on-line color version. Bright (red) means strong intensity. The color map is logarithmically scaled.

The main arc crossing the figure is the electron rotation frequency. This rotation frequency is the "dressed" field-free rotation frequency of the electron orbit. The laser field correction is the analog of the ac Stark effect. The other arcs are reminiscent of the strong hyper Raman lines. The vertical lines on the left part of the figure are odd laser harmonics. Note that the arcs are many order of magnitudes weaker than the harmonic lines [see Figs. 2(a) and 4(b)]. The completely white bands correspond to trajectories which immediately ionize. The ionization observed is the classical "over the barrier" ionization. In our simulation, once an electron is ionized it never returns to the atom (this is because the assumption of zero momentum after tunneling made in the three-step model does not apply here). On the border between bound motion and ionization, there is a very narrow slice of initial conditions that generates (bound) chaotic motion. This was verified by observation of positive Lyponov exponents for these trajectories. Chaotic motion can be suppressed by quantum mechanics [19], so we exclude and disregard the spectra of chaotic trajectories.

While the first few harmonics appear for all r_0, it is only a few isolated radii that give rise to the higher harmonics. Notice that some of these points occur when the rotation arc and vertical odd harmonic lines cross. This effect is easily understood using the "sampling" effect discussed in the previous subsection [Fig. 2(b)]. Below the cutoff, the ensemble spectrum samples the one member spectrum in frequencies which are the odd laser harmonics. Therefore, if the single member has its peaks exactly at these points, the ensemble spectrum will have strong "samples." This is in complete agreement with Ref. [12] where this effect was first observed. It is important to note that there are other dominant points in the spectrum for which the rotation arc does not cross a laser harmonic vertical line (e.g., $r_0 = 1.82$, $r_0 = 1.95$). Their origin is not clear yet.

In the second band, there are some trajectories (close to the chaotic ones) whose peaks in the spectrum are slightly shifted from the expected odd laser harmonics. This effect can also be observed in a simple one-dimensional anharmonic oscillator. In one dimension, a tiny friction effect is enough to put the peaks back in place.

We point out that in one dimension, the spatial origin of the radiation is not a well-defined concept. Trying to isolate the zone of radiation (say by a Gabor transformation) seriously distorts the spectrum. In two dimensions, the electron motion is around the initial radius (up to 15% of the radius for strong fields) so one can tell which are the more active zones in the atom. Moreover in terms of field-free initial conditions (namely, r_0) the radiation origin in two-dimensions can be spatially located even more precisely. This can be seen in Fig. 3, which suggests that HHG originates from small a number of circular ensembles. The $5p$ wave function extends until a radius of about 5 a.u., yet the classical HHG hot spots constitute less than 3% of that distance.

C. Sampling theorem and ensemble integration

Since the acceleration $\ddot{x}(t,\varphi)$ is periodic in φ, it can be written as

$$\ddot{x}(t,\varphi) = \sum_k a(t,k)\exp(\imath k\varphi), \tag{6}$$

where $a(t,k)$ are complex coefficients, and$k$ is the azimuthal frequency. After averaging over φ to get the ensemble acceleration, only the $k = 0$ term remains. This, however, is no longer correct when the continuous integration is replaced by an M points sum. The sampling theorem states that azimuthal frequencies higher than $M/2$ will be "folded" or shifted to a lower frequency. Specifically, the $k = M, 2M, 3M, \ldots$, frequencies will be folded to $k = 0$. All frequencies which fold into nonzero frequencies will cancel out in the ensemble sum, but the terms that were folded to zero will remain and appear as an artifact in the ensemble spectrum.

In Fig. 4(a), the two-dimensional Fourier transform of $\ddot{x}(t,\varphi)$ [i.e., $a(\omega,k)$] is plotted. Each curve corresponds to a different azimuthal frequency, and the x axis is the temporal frequency in units of laser harmonics. The strongest peak, located at $\omega = 7.72\omega_L$, is the rotation frequency. The peak of the kth azimuthal frequency is at $\sim kM\omega_{\text{rotation}} \sim kM\omega_{\text{ff}}$. From the figure, it is clear that if the Mth component is folded to $k = 0$, then the peak of the artifact will appear at multiples of

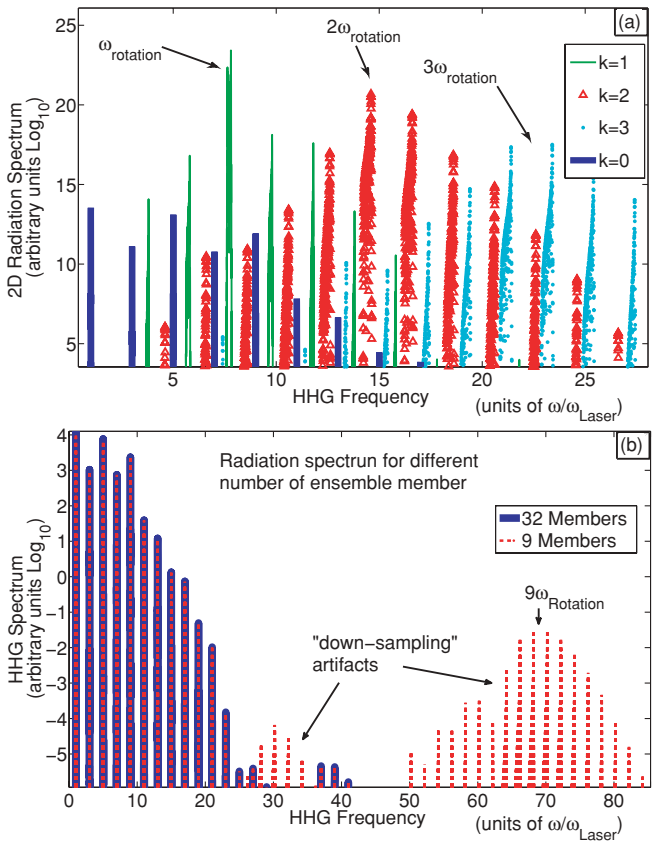

FIG. 4. (Color online) (a) The two-dimensional Fourier transform over time and initial angle of the electron acceleration. The spectrum is discrete in the azimuthal frequency. The kth marker corresponds to the kth azimuthal frequency number. For very large M, only the zeroth component survives the ensemble average and contributes to HHG. (b) for $M = 9$ (thin red line) ensemble members, and the same parameter as in Fig. 1, the artifacts centered around $9\omega_{\text{rotation}}$ are the results of the $k = 9$ spectrum being folded onto $k = 0$ according to the sampling theorem. If more ensemble members are considered, the low-frequency zone remains the same but the artifacts are pushed to higher frequencies. For comparison, the thick (blue) line is 32 ensemble members.

$kM\omega_{\text{ff}}$ (often the second multiple is already too weak to be observed).

For example, if the ensemble spectrum of Fig. 1(b) is calculated using only four points, the spectrum will look like a superposition of $k = 0$ [of Fig. 4(a)] and $k = 4$. By choosing larger M, the artifacts can be pushed farther and farther to higher frequencies away from the zone of interest. To illustrate this, Fig. 4(b) shows the spectrum for $M = 9$ and for $M = 32$ ensemble members. Notice that the artifact appears only in the high frequencies around $9\omega_{\text{rotation}} \sim 9\omega_{\text{ff}}$ and that in the low zone the two spectra are identical as expected from the sampling theorem. Consequently, the calculations converge to the correct result beyond a critical member number, and a further increase of the ensemble size does not improve the accuracy. Let $\omega_{\max}$ be the highest frequency of interest in the system. The critical value of M, for which the artifact is located at $\omega_{\max}$, is given by $M_{\text{crit}} > \omega_{\max}/\omega_{\text{ff}}$. In practice because of the spectral width of the artifact, usually a slightly larger value is taken. For xenon, M can be taken to be as small as 16; and closer to the core where ω_R is higher, it can be even less. This understanding may lead to a simplification of the classical scheme and substantial reduction of the needed computer resources.

D. Seeding

Fleischer and Moiseyev [17] considered a one-dimensional quantum forced oscillator that in addition to the standard laser pulse excitation, a very weak "seed" pulse, of much higher frequency was added. They showed that a HHG spike pattern of $2\omega_L$ spacing emerges around the seed's frequency. Calculating

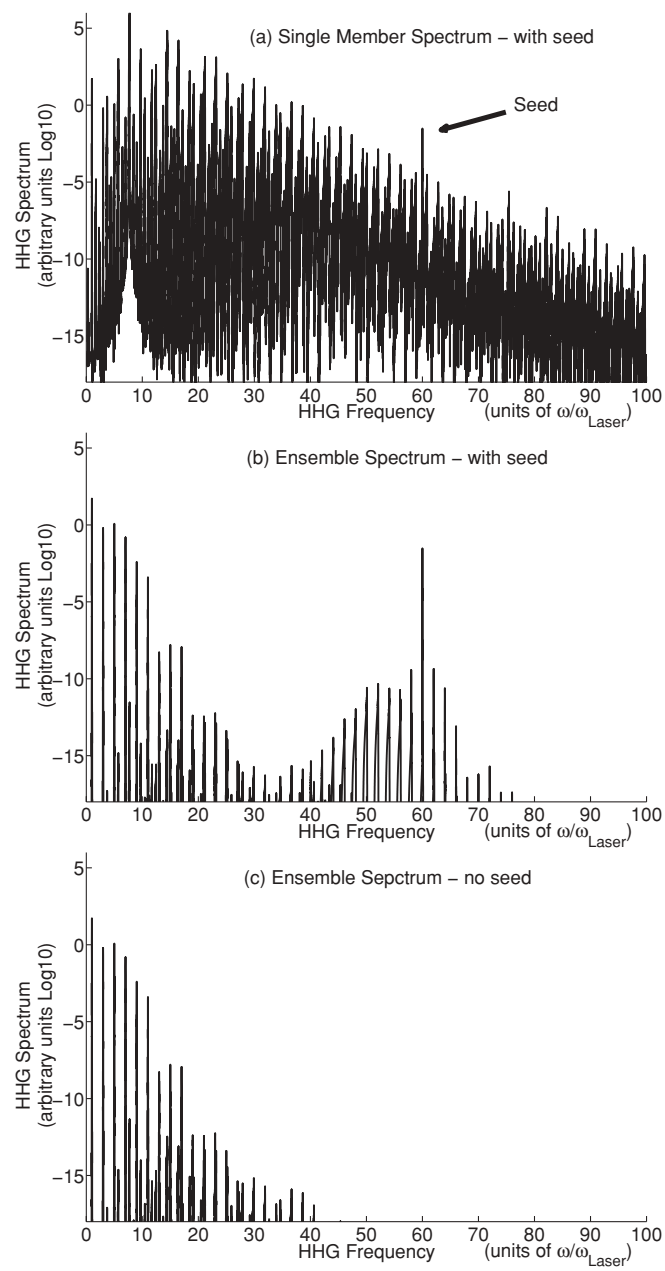

FIG. 5. (a) A typical single member "seeded" HHG spectrum for $I_{\text{laser}} = 3 \times 10^{13}$ W/cm^2, $I_{\text{seed}} = 3 \times 10^8$ W/cm^2. The seed signal is hardly visible. (b) After doing the ensemble average, a comb pattern of $2\omega_{\text{laser}}$ spacing appear as in Ref [17]. (c) For comparison, the ensemble average without seed is plotted.

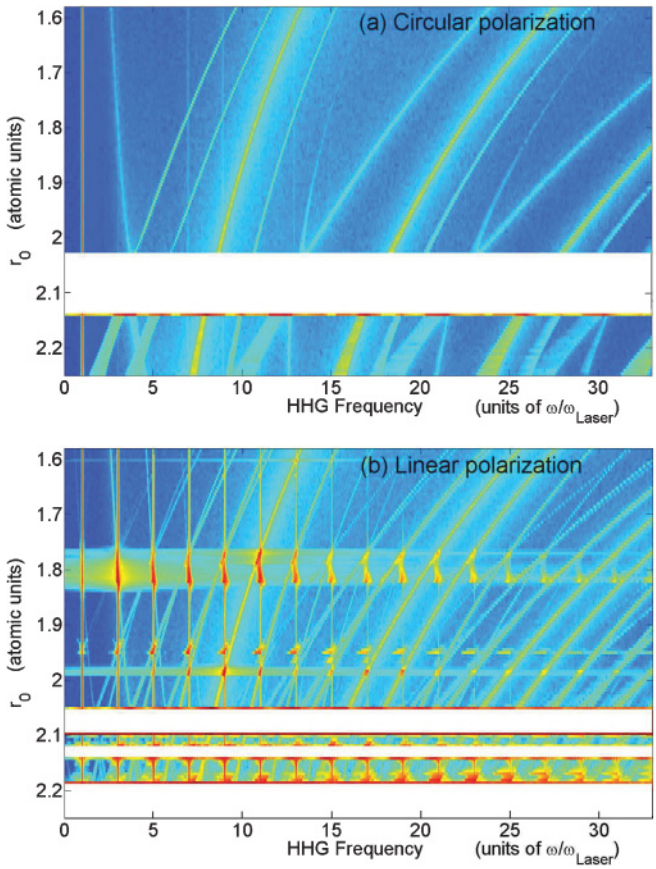

FIG. 6. (Color online) The HHG spectrum (x axis) as a function of r_0, the distance from the nucleus (y axis), is shown for (a) circular polarization and (b) linear polarization. The field strength is the same as in Fig. 3 for both cases. [Plot (b) is the same as Fig. 3. It was plotted again for comparison.] There are no vertical lines of odd harmonics and no hot spots of HHG for circular polarization. The reason for the effect is different from that provided by the three-step model.

the classical ensemble spectrum for such excitation, a very similar result appears. In Fig. 5(a), the HHG spectrum was calculated for the following parameters: $r_0 = 2.16$ a.u., $I_{\text{laser}} = 3 \times 10^{13}\ \text{W/cm}^2$, $I_{\text{seed}} = 3 \times 10^8\ \text{W/cm}^2$, and $\omega_{\text{seed}} = 60\omega_{\text{laser}}$. One can see in Fig. 5(a) that for the single member spectrum, the seed is almost unobservable. Yet, after taking the ensemble average (50 points were enough) a clear "comb" pattern emerges. The quantum results are for a one-dimensional case, so there is no point in quantitative comparison. The classical seeding can be easily understood by treating the seed as a small perturbation in the accelerated system defined by $x_{\text{new}} = x_{\text{old}} - \int dt^2[A_L(t)\sin(\omega_L t) + A_{\text{seed}}(t)\sin(\omega_{\text{seed}} t)]$. A simple Taylor expansion shows there are *even* laser harmonics centered around ω_{seed}.

E. Circular polarization

For circular polarization in radially symmetric atoms or molecules, the HHG spectrum is highly attenuated with respect to linear polarization [6]. In quantum mechanics, the reason for this attenuation can be attributed to the symmetry properties of the Hamiltonian [20]. In the strong field approximation, the three-step-model explanation is that the electron misses the core and only the tail of the wave packet hits the nucleus and causes some radiation. For the intensities discussed here, however, the orbits are roughly circular for both polarizations. Nonetheless, we find that in our model, HHG radiation is practically zero for circular polarization. Figure 6(a) shows the ensemble spectra for different initial radii. Except for the first harmonic, no harmonic lines appear at all. The laser field amplitude is identical to the linear case shown in Fig. 3. For a convenient comparison the linear polarization case is plotted in Fig. 6(b). The single member spectrum of the circular polarization is comparable to that of the linear polarization. In the linear case, however, constructive interference was observed for odd harmonics [Fig. 2(b)], while for circular polarization there is no such "phase clamping." This phase mechanism is very different from the "missing the core" argument in which each trajectory hardly radiates.

IV. CONCLUSION

In this work it was demonstrated how the known generic features of a high-harmonic spectrum emerge by averaging over different evenly spaced initial conditions. The fact that the ensemble average spectrum is a "sampled" version of the single member spectrum explains some of the "hot spots" in classical HHG. In addition, for xenon atoms, it was found that the classically active HHG zones are a small faction ($\sim$3%) of the extent of the initial-state wave function. The sampling theorem was used to show that very few ensemble members are needed to get accurate results if a uniform grid is used for the initial condition angle. This result is not true if the standard Monte Carlo approach is taken.

The classical origin of seeding and circular polarization effects were discussed and the dramatic impact of the ensemble average was once more demonstrated. The "ensemble effect" in all the examples, is attributed to the relative phase between ensemble members, and not to the spectral shapes of the radiation of individual members.

ACKNOWLEDGMENTS

Support by the ISF Grant 96/07 is acknowledged. R.U. thanks the B.L. Maas research fund for its support.

[1] A. L'Hullier, K. J. Schafer, and K. C. Kulander, J. Phys. B **24**, 3315 (1991).
[2] M. Protopapas, C. H. Keitel, and P. L. Knight, Rep. Prog. Phys. **60**, 389 (1997).
[3] J. G. Eden, Prog. Quantum Electron. **28**, 197 (2004).
[4] X. F. Li, A. L'Huillier, M. Ferray, L. A. Lompre, and G. Mainfray, Phys. Rev. A **39**, 5751 (1989).
[5] A. L'Huillier and Ph. Balcou, Phys. Rev. Lett. **70**, 774 (1993).
[6] K. S. Budil, P. Salieres, Anne L'Huillier, T. Ditmire, and M. D. Perry, Phys. Rev. A **48**, R3437 (1993).

[7] P. B. Corkum, Phys. Rev. Lett. **71**, 1994 (1993).
[8] M. Lewenstein, Ph. Balcou, M. Y. Ivanov, A. L'Huillier, and P. B. Corkum, Phys. Rev. A **49**, 2117 (1994).
[9] G. van de Sand and J. M. Rost, Phys. Rev. Lett. **83**, 524 (1999).
[10] J. G. Leopold and I. C. Percival, J. Phys. B **12**, 709 (1979).
[11] Y. Duan, W. K. Liu, and J. M. Yuan, Phys. Rev. A **61**, 053403 (2000).
[12] G. Bandarage, A. Maquet, T. Menis, R. Taieb, V. Veniard, and J. Cooper, Phys. Rev. A **46**, 380 (1992).
[13] P. Botheron and B. Pons, Phys. Rev. A **80**, 023402 (2009).
[14] C. H. Keitel and P. L. Knight, Phys. Rev. A **51**, 1420 (1995).
[15] S. Chu, K. Wang, and E. Layton, J. Opt. Soc. Am. B **7**, 425 (1990).
[16] K. C. Kulander and B. W. Shore, J. Opt. Soc. Am. B **7**, 502 (1990).
[17] A. Fleischer and N. Moiseyev, Phys. Rev. A **77**, 010102(R) (2008).
[18] Ph. Balcou, A. L'Huillier, and D. Escande, Phys. Rev. A **53**, 3456 (1996).
[19] H. J. Korsch and M. V. Berry, Physica D (Amsterdam) **3**, 627 (1981).
[20] O. E. Alon, V. Averbukh, and N. Moiseyev, Phys. Rev. Lett. **80**, 3743 (1998).